Highly transparent tactile sensor based on a percolated carbon nanotube network

Yongwoo Lee, Bongsik Choi, Jinsu Yoon, Yeamin Kim, Jinhee Park, Hyo-Jin Kim, Dae Hwan Kim, Dong Myong Kim, Sungho Kim, and Sung-Jin Choi

Highly transparent tactile sensor based on a percolated carbon nanotube network

Yongwoo Lee,[1] Bongsik Choi,[1] Jinsu Yoon,[1] Yeamin Kim,[1] Jinhee Park,[1] Hyo-Jin Kim,[1] Dae Hwan Kim,[1] Dong Myong Kim,[1] Sungho Kim,[2,a] and Sung-Jin Choi[1,a]

[1]*School of Electrical Engineering, Kookmin University, Seoul 02707, Korea*
[2]*Department of Electrical Engineering, Sejong University, Seoul 05006, Korea*

The demand for transparent and flexible electronic devices, which are an emerging technology for the next generation of sensors, continues to grow in both applications and development due to their potential to make a significant commercial impact in a wide variety of areas. Here, we demonstrate a highly transparent tactile sensor with 92% optical transparency in the visible range based on solution-processed 99% metallic CNTs attached on a polydimethylsiloxane (PDMS) film. We efficiently reconstructed the pressed, stimulated spatial location by increasing the injection current ($I_{injection}$) during electrical resistance tomography (ERT) that computed the internal two-dimensional (2-D) resistivity distribution. © *2018 Author(s).*
All article content, except where otherwise noted, is licensed under a Creative Commons Attribution (CC BY) license (http://creativecommons.org/licenses/by/4.0/).
https://doi.org/10.1063/1.5036530

Various types of discrete sensors, such as strain sensors or piezoelectric transducers, have been used for detecting regions of damage in real time in applications including civil aviation, spacecraft, military vehicles, automobiles, other transportation systems, and pressure vessels. However, many of these sensors, including those reported in the literature, were inherently complicated, incurred a weight penalty due to the weight of discrete sensors, and required complex wiring.[1] Therefore, electrical resistance tomography (ERT) has been introduced as an alternative solution to overcome the aforementioned limitations in detecting and diagnosing regions of damage and in enabling high-performance image sensing in a non-destructive manner in real time without any complicated wiring.[2–4] ERT is a technique that computes internal resistivity (or conductivity) distribution from a continuum conductive model using simple electrodes that are fabricated along the boundary of the conductive material. Changes in resistivity at various locations introduced by damage are readily measured by applying electrical currents to the conductive film. The damaged spatial location and its magnitude are predicted by solving the inverse problem based on the electrical measurement.[1,2,5–8] Due to this easy detection method, ERT could also be employed as strain gauges for sensing purposes in several innovative fields such as biomedicine and healthcare.[9–15] In particular, ERT has been regarded as a strong candidate technology for use as a tactile sensor for sensitive electronic skin applications because it does not need any internal complicated wiring.

Recently, carbon nanotubes (CNTs) have been extensively studied as flexible electronic devices, sensors, and biomaterials because of their excellent mechanical, electrical, chemical, and thermal properties.[16–20] Owing to these superior material properties, CNTs are one of the emerging materials that have proven their applicability as various sensors, including tactile sensors.[21–25] Several groups have reported the spatial characterization of the resistivity in CNT-based thin films using ERT for detecting the extent of damage,[26,27] for distinguishing pH changes,[13,28] and for use as tactile sensors. However, until now, there have been few reports on the ERT-based tactile sensor composed of CNTs

[a]Electronic addresses: sjchoiee@kookmin.ac.kr & sungho85kim@sejong.ac.kr. Tel.: +82-2-910-5543. Fax: +82-2-910-4449.

with both satisfactory electrical characteristics and high optical transparency. In recent decades, there have been tremendous advances in an effort to obtain high-purity CNTs through the solution-based purification process (i.e., ultracentrifugation process), which allows CNTs to be rapidly and inexpensively separated according to their electronic type: semiconducting or metallic.[29,30] In particular, electronic devices with record-breaking performance have been fabricated using solution-based CNTs with greater than 99% semiconducting purity.[31–33] It has also been reported that high-purity metallic CNTs are more suitable for superior optical transparency because poorly conducting, strongly absorbing carbonaceous impurities, and semiconducting CNTs were eliminated through the density-gradient ultracentrifugation (DGU) process;[34,35] hence, high-purity metallic CNTs would be a good choice for use in the ERT-based tactile sensor with excellent optical transparency and high electrical performances for an aesthetic view of human applications.

The present work demonstrates a highly transparent ERT-based tactile sensor based on solution-processed 99% metallic CNTs adhered to polydimethylsiloxane (PDMS). We fabricated a highly conductive and transparent percolated network using metallic CNTs with high optical transparency of over 92% in the visible range. The percolated network of metallic CNTs was formed directly on a PDMS substrate using an easy, scalable, and low-cost spray-coating method. We investigated the mapping responses by the spatial resistivity changes, using ERT to evaluate the performance of the solution-processed metallic CNT-based tactile sensor. Our transparent film exhibited piezoresistivity due to the morphological changes of the metallic CNT percolation network along the direction of the pressure.[15,35–37] In particular, we focused on implementing efficient image reconstruction of the pressed position on our highly transparent tactile sensor by increasing the injection current ($I_{injection}$) to the outer electrodes when using ERT. We found that by increasing $I_{injection}$, the resolution of the internal resistivity profile of the tactile sensor based on metallic CNT networks was improved when comparing the actual pressed area and the image reconstruction area.[27]

Figure 1a shows the schematic diagram of the ERT measurement system. ERT reconstructs a two-dimensional (2-D) spatial resistivity distribution using the input-output current-voltage measurement method at the boundary of the conductive material. An adjacent ERT measurement requires a total of four electrodes, which must be set as follows: inject current into one electrode, another electrode to ground, and the other two electrodes to measure the voltage difference. The electrodes of the metallic CNT-PDMS film in this study were electrically interconnected with a copper alligator clip at the boundary. The electrical measurement was performed by a semiconductor parameter analyzer (Agilent 4156C) for applying a direct current (DC) source and measuring the output voltage difference and the switch mainframe (E5250A, Agilent) for sequential input-output current-voltage
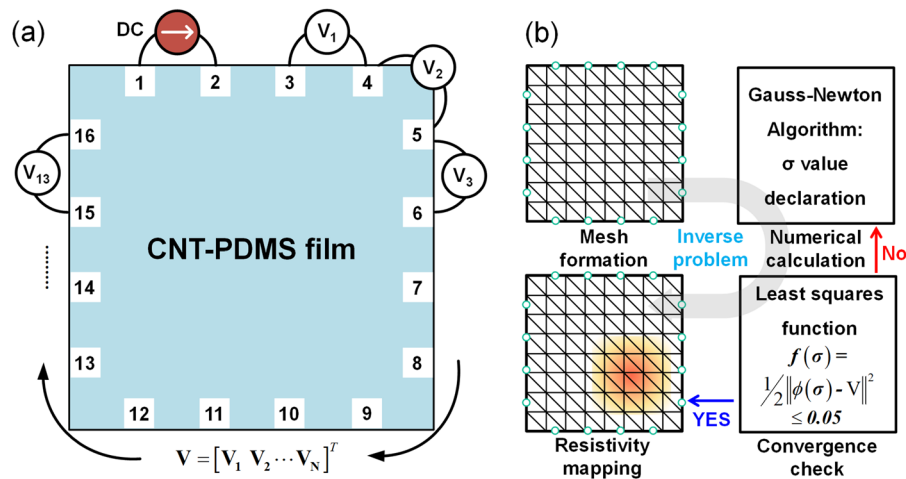

FIG. 1. (a) A schematic showing a measurement system for an adjacent ERT method for imaging a square-shaped CNT-PDMS film with 16 electrodes. (b) A schematic illustrating the ERT spatial resistivity reconstruction process. To solve for the spatial resistivity distribution, an iterative process utilizing a finite element model is used to solve the inverse problem until the solution converges.

measurements. Obtaining two sets of voltage value series before and after a stimulus that causes a resistance change in an adjacent method provides the basis for reconstructing the spatial resistivity distribution.[5–7,9–13] An overview schematic of the ERT processes showing the spatial resistivity distribution is shown in Figure 1b. In general, the ERT technique for reconstructing the spatial resistivity distribution uses MATLAB simulation and the inverse problem, which is an iterative reconstruction algorithm calculation.[5–8] The inverse problem is a model that determines the spatial resistivity distribution of an unknown material based on numerous input-output experimental boundary electrode measurements.

For the transparent, conductive CNT-percolated film in an ERT-based tactile sensor, we produced the percolated network of the solution-processed 99% metallic CNTs on a thin PDMS substrate.[35] Figure 2a shows the spray-coating method for the 99% metallic CNT networks directly on the PDMS layer. The tactile sensor fabrication processes are briefly explained as follows. First, a flexible and transparent 1-mm-thick PDMS substrate was prepared by mixing PDMS prepolymer (Sylgard 184A, Dow Corning) and a curing agent in a ratio of 10:1 by weight. Next, the substrate was cleaned by oxygen plasma treatment and then functionalized with a poly-L-lysine solution (0.1% w/v in H_2O; Sigma Aldrich) that acts as an effective adhesion layer for the deposition of the 99% metallic CNTs. The substrate was thoroughly rinsed with deionized (DI) water and dried with flowing nitrogen gas. Subsequently, the transparent metallic CNT network film was directly formed on the PDMS substrate by spray coating (150 spray coats) the pre-separated, metallic CNT solution (high metallic purity (99%) and a concentration of 0.01 mg/mL) on a hot plate at 100 °C, followed by thorough rinsing with isopropanol and DI water. Note that the spray-coating method is a facile and low-cost fabrication that can easily form the CNT percolated network on any large area substrate with high throughput. Moreover, the density of the CNT network film can be easily controlled to tune the performance of the sensor. As a final step, the substrate was annealed at 100 °C for an hour.

Figure 2b shows the image of the PDMS layer that was spray coated with 99% metallic CNTs with great flexibility and transparency. It is worthwhile to note that the percolated CNT network film
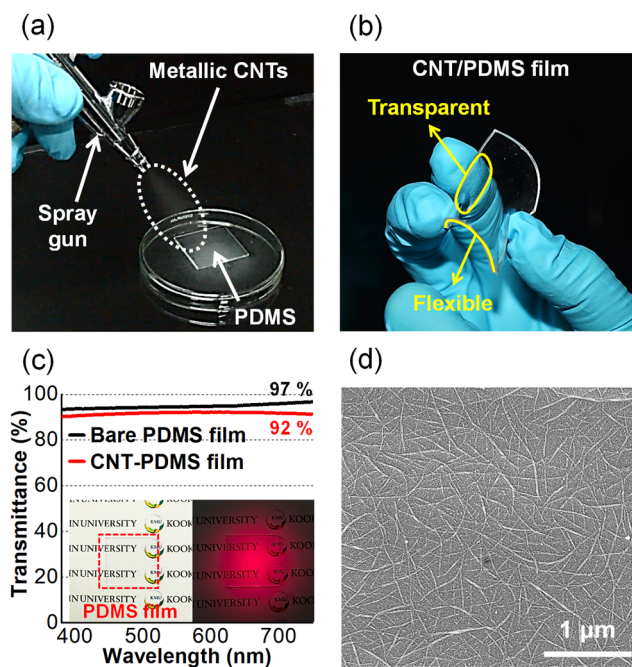

FIG. 2. (a) An image showing that a highly purified, pre-separated, 99% metallic CNT solution is spray coated on the PDMS layer during the sensor fabricating process. (b) An image of the fabricated metallic CNT-based tactile sensor with great flexibility and transparency. (c) Optical transparency of the bare PDMS film and the metallic CNT-PDMS film with 150 spray coats in the visible range. An image of the tactile sensor in bright or dark environments. (d) SEM images showing the 150 spray-coated metallic CNT networks on the PDMS.

formed by highly purified, solution-processed 99% metallic CNTs shows high optical transparency. Figure 2c shows the measured optical transparency of the CNT percolated film with greater than 92% in the visible range using a UV/Vis/NIR spectrophotometer (Cary 5000, Agilent), even though we used a large number of sprays for implementation of a highly conductive film (150 spray coats). Moreover, a reduction of only 5% in optical transparency was obtained compared to the bare PDMS. The transparency of the film was sufficient to render characters legible on background paper even in bright or dark environments. Until recently, the previously reported tactile sensors were based on carbon compound materials or a percolated network of CNTs and were generally opaque. However, our tactile sensors have a wider range of applications in terms of high transparency due to the advantages of highly purified, solution-processed metallic CNTs from the DGU process. In particular, electronic devices with high transparency,[35] including our tactile sensors, can be sufficiently utilized in human or smart display applications. Moreover, the scanning electron microscope (SEM) images of the percolated CNT network, as shown in Figure 2d, were found to be dense and uniform across the entire area, which is critical for reducing the variation of the sensing response and improving the sensing performance. The average CNT density obtained for 150 spray coats of the 99% metallic CNT solution was extracted as approximately 86 ± 3 tubes/μm^2.

A total of 16 copper alligator clips were used to connect the electrodes to the metallic CNT network film; then, a total of 208 values of the voltage difference were collected through the adjacent ERT method. As shown in Figure 3a, a large PDMS frame was made to hold the copper alligator clips in place to minimize micro-shaking of the contact between the PDMS and electrodes. An adjacent ERT measurement requires a pair of voltage measurements (before and after stimulation). Therefore, an ERT mapping image can be reconstructed by acquiring $208 \times 2 = 416$ voltage measurements. Thus, in the adjacent method, the reconstructed image through ERT shows the rate of change of the relative resistivity value, not the rate of change of the absolute resistivity value. In addition, the reconstructed image is composed by the finite element method (6400 mesh elements in our work), and the change rate of the resistivity calculated approximately for each element is shown as a 2-D image.
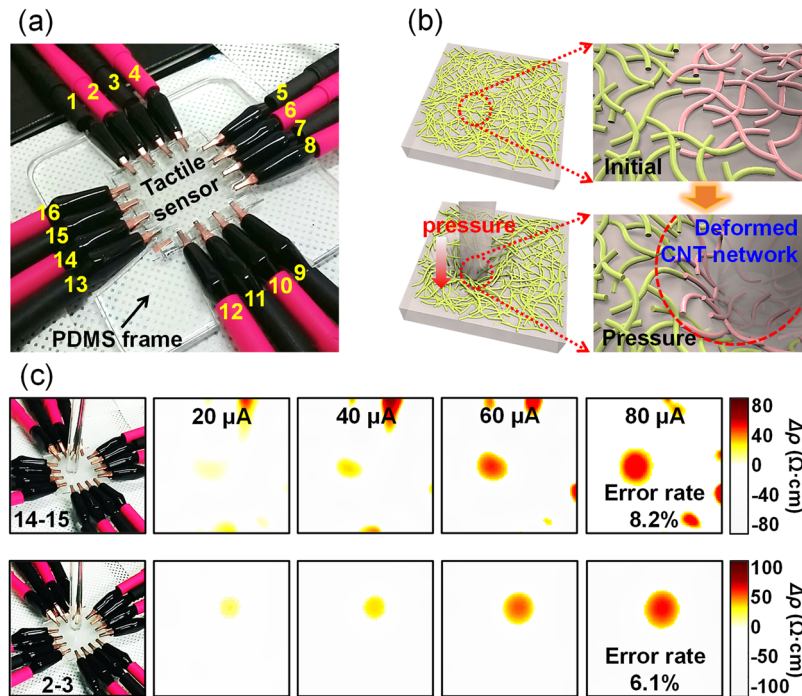

FIG. 3. (a) A real ERT measurement image of a tactile sensor with a copper alligator clip to connect to the metallic CNT networks on the PDMS. (b) Illustration of a CNT network formed on the PDMS before and after pressure is induced. (c) The reconstructed images that are shown through the ERT measurements according to the different $I_{injection}$ of the fabricated tactile sensor.

Note that the number of electrodes was arbitrarily set from 1 to 16 in order to determine the position where the pressure was applied. The performance of our squared-shaped ERT-based tactile sensor (30 mm × 30 mm) was tested using a 3.8-mm radius glass rod for applying constant pressure (62 kPa) at designated locations. The pressure was applied to the CNT networked film alternatively at positions between electrodes 14 and 15 and between electrodes 2 and 3. The resistance of the stimulated part of the metallic CNT-based tactile sensor was expected to increase by the morphological deformation of the percolated metallic CNT network; that is, in the stimulated part, the CNT network was loosened, resulting in a reduced current path and an increased spatial resistance, as schematically shown in Figure 3b. This is a well-known mechanism in network-based strain sensors composed of one-dimensional materials such as CNTs.[35,38] To verify the sensing performance of metallic CNT-based tactile sensor, the ERT measurements were performed under various $I_{injection}$ ranging from 20 to 80 μA to investigate the sensing response, as shown in Figure 3c. The best resolution spatial mapping image under the same applied pressure was reconstructed at the highest $I_{injection}$ of 80 μA because the highest $I_{injection}$ results in the largest potential difference. At this time, the estimated maximum resistivity change of the fabricated metallic CNT-based tactile sensor was extracted as 49.4 Ω·cm. In addition, the results showed that the error rate for the pressure response of our metallic CNT-based tactile sensor decreased by up to 6.1% for compared to the actual pressed area by the glass rod. However, unwanted images were also reconstructed near other electrodes due to measurement artifacts, such as micro-shaking of the contact between the CNT network during ERT measurements or the incompleteness of the one-dimensional segment model of the electrodes in the forward model.[39] As $I_{injection}$ decreases, the pressure response of the reconstructed images begins to fade, and eventually the pressure response is hardly recognizable at the lowest $I_{injection}$ (20 μA). Our metallic CNT-based tactile sensor detects the accurately matched location with spatial stimulus because we use a spray-coating method that can uniformly and stably deposit the high-density metallic CNT film (150 sprays). From these results, we were able to obtain a high-resolution reconstructed image using ERT that can perform 2-D spatial resistivity change mapping by appropriately adjusting the $I_{injection}$ for the ERT measurements. Although we did not additionally measure the multiple pressure response induced by the simultaneous pressure of various shapes or the tactile response for the electronic skin, we believe that the distinguishable responses of stable and high-resolution sensors on the skin will enable human applications and smart displays.

In conclusion, we demonstrate a transparent tactile sensor based on solution-processed 99% metallic CNTs with high-density using a facile spray-coating method. In particular, tactile sensors based on high-purity metallic CNTs with reduced carbonaceous impurities that are poorly conducting and strongly absorbing through the DGU process, achieved a high optical transparency of over 92% in the visible range. In addition, the fabricated transparent tactile sensor was evaluated for resolution at a constant pressure using the ERT technique, which partially computes the internal resistivity change. Applying high $I_{injection}$ into the tactile sensor creates a high potential difference from constant pressure; thus, the reconstructed ERT image is clearly detected. In other words, acceptable sensing performance is controlled by the different $I_{injection}$ values of the tactile sensor. Therefore, we believe that our results will provide a significant turning point towards a transparent future for the sensor market.

[1] R. W. Ross and Y. L. Hinton, AIAA/ASME/ASCE/AHS/ASC Structures, Structural Dynamics and Materials Conference, p. 1936 (2008).
[2] L. Borcea, Inverse Problems **18**, R99 (2002).
[3] A. D. Seagar, IEE Proceedings A **134**, 201 (1987).
[4] R. W. M. Smith, I. L. Freeston, and B. H. Brown, IEEE Trans. Biomed. Eng. **42**, 133 (1995).
[5] M. Vauhkonen, W. R. B. Lionheart, L. M. Heikkinen, P. J. Vauhkonen, and J. P. Kaipio, Physiol. Meas. **22**, 107 (2001).
[6] N. Polydorides and W. R. B. Lionheart, Meas. Sci. Technol. **13**, 1871 (2002).
[7] B. M. Graham and A. Adler, Int. J. Information Syst. Sci. **2**, 435 (2006).
[8] B. R. Loyola, V. La Saponara, K. J. Loh, T. M. Briggs, G. O'Bryan, and J. L. Skinner, IEEE Sens. J. **13**, 2357 (2013).
[9] K. J. Loh, T.-C. Hou, J. P. Lynch, and N. A. Kotov, J. Nondestruct. Eval. **28**, 9 (2009).

[10] A. Romsauerova, A. McEwan, L. Horesh, R. Yerworth, R. H. Bayford, and D. S. Holder, Physiol. Meas. **27**, S147 (2006).

[11] B. Grychtol and A. Adler, Physiol. Meas. **34**, 579 (2013).

[12] T. Sun, S. Tsuda, K.-P. Zauner, and H. Morgan, Biosens. Bioelectron. **25**, 1109 (2010).

[13] T.-C. Hou, K. J. Loh, and J. P. Lynch, Nanotechnology **18**, 315501 (2007).

[14] G. H. Büscher, R. Kõiva, C. Schürmann, R. Haschke, and H. J. Ritter, Rob. Auton. Syst. **63**, 244 (2015).

[15] H. Lee, D. Kwon, H. Cho, I. Park, and J. Kim, Sci. Rep. **7**, 39837 (2017).

[16] L. Cai, S. Zhang, J. Miao, Z. Yu, and C. Wang, ACS Nano **10**, 11459 (2016).

[17] S. Zhang, L. Cai, T. Wang, R. Shi, J. Miao, L. Wei, Y. Chen, N. Sepúlveda, and C. Wang, Sci. Rep. **5**, 17883 (2016).

[18] T. Yamada, Y. Hayamizu, Y. Yamamoto, Y. Yomogida, A. Izadi-Najafabadi, D. N. Futaba, and K. Hata, Nat. Nanotechnol. **6**, 296 (2011).

[19] X. Cao, F. Wu, C. Lau, Y. Liu, Q. Liu, and C. Zhou, ACS Nano **11**, 2008 (2017).

[20] T. S. Gspann, S. M. Juckes, J. F. Niven, M. B. Johnson, J. A. Elliott, M. A. White, and A. H. Windle, Carbon **114**, 160 (2017).

[21] H. Li, C. Wen, Y. Zhang, D. Wu, S.-L. Zhang, and Z.-J. Qiu, Sci. Rep. **6**, 21313 (2016).

[22] J.-W. Han, B. Kim, J. Li, and M. Meyyappan, J. Phys. Chem. C **116**, 22094 (2012).

[23] C. Yeom, K. Chen, D. Kiriya, Z. Yu, G. Cho, and A. Javey, Adv. Mater. **27**, 1561 (2015).

[24] J. Li, Y. Lu, Q. Ye, M. Cinke, J. Han, and M. Meyyappan, Nano Lett. **3**, 929 (2003).

[25] Q.-Y. Tang, Y. C. Chan, and K. Zhang, Sensors Actuators B Chem. **152**, 99 (2011).

[26] A. Baltopoulos, N. Polydorides, L. Pambaguian, A. Vavouliotis, and V. Kostopoulos, J. Compos. Mater. **47**, 3285 (2013).

[27] B. Kim, Y. Lu, T. Kim, J.-W. Han, M. Meyyappan, and J. Li, ACS Nano **8**, 12092 (2014).

[28] K. J. Loh, J. Kim, J. P. Lynch, N. W. S. Kam, and N. A. Kotov, Smart Mater. Struct. **16**, 429 (2007).

[29] M. S. Arnold, S. I. Stupp, and M. C. Hersam, Nano Lett. **5**, 713 (2005).

[30] M. S. Arnold, A. A. Green, J. F. Hulvat, S. I. Stupp, and M. C. Hersam, Nat. Nanotechnol. **1**, 60 (2006).

[31] C. Qiu, Z. Zhang, M. Xiao, Y. Yang, D. Zhong, and L.-M. Peng, Science **355**, 271 (2017).

[32] G. S. Tulevski, A. D. Franklin, D. Frank, J. M. Lobez, Q. Cao, H. Park, A. Afzali, S.-J. Han, J. B. Hannon, and W. Haensch, ACS Nano **8**, 8730 (2014).

[33] S.-J. Choi, P. Bennett, K. Takei, C. Wang, C. C. Lo, A. Javey, and J. Bokor, ACS Nano **7**, 798 (2013).

[34] A. A. Green and M. C. Hersam, Nano Lett. **8**, 1417 (2008).

[35] J. Lee, M. Lim, J. Yoon, M. S. Kim, B. Choi, D. M. Kim, D. H. Kim, I. Park, and S.-J. Choi, ACS Appl. Mater. Interfaces **9**, 26279 (2017).

[36] S. Li, J. G. Park, Z. Liang, T. Siegrist, T. Liu, M. Zhang, Q. Cheng, B. Wang, and C. Zhang, Carbon **50**, 3859 (2012).

[37] S. C. B. Mannsfeld, B. C.-K. Tee, R. M. Stoltenberg, C. V. H.-H. Chen, S. Barman, B. V. O. Muir, A. N. Sokolov, C. Reese, and Z. Bao, Nat. Mater. **9**, 859 (2010).

[38] A. V. Tobolsky, J. Appl. Phys. **27**, 673 (1956).

[39] A. Adler and W. R. B. Lionheart, Physiol. Meas. **27**, S25 (2006).